"A Cochlear Nucleus Auditory prosthesis based on microstimulation"

Contract No. **No. NO1-DC-1-2105**
Progress Report #10

HUNTINGTON MEDICAL RESEARCH INSTITUTES
NEURAL ENGINEERING LABORATORY
734 Fairmount Avenue
Pasadena, California 91105

D.B. McCreery, Ph.D.
L.A. Bullara, B.S.
A.S. Lossinsky, Ph.D.

HOUSE EAR INSTITUTE
2100 WEST THIRD STREET
Los Angeles, California 90057

R.V. Shannon Ph.D
S. Otto M.S.
M. Waring, Ph.D

INTRODUCTION & ABSTRACT

After reviewing the intraoperative video from the first patient to receive the penetrating auditory brainstem implant array (PABI), we concluded that the placement of the penetrating array was a bit too caudal. We therefor elected to implant the array in PABI patient #2 in a slightly superior location, just dorsal to the root of the VIII nerve, and into the lateral wall of the nucleus, just dorsal of the taenia choroidia.

When PABI patient #2 returned for her hook-up 6 weeks after the surgery, she was getting good auditory sensations with low thresholds (1.7 nC/phase or below) from 5 of the 8 penetrating electrodes. One penetrating electrode induced dizziness at low stimulus amplitude, and the thresholds of the auditory percepts from two penetrating electrodes were close to the 3 nC/safety limits; they appear to be on the edge of the cochlear nucleus. She is perceiving a wide range of pitches (from 15 to 80 on a scale of 0 to 100) from the other 5 penetrating microelectrodes, and has a full range of loudness percepts, ranging from faint to loud, on all 5 channels, without exceeding the 3 nC/phase safety limit, and with no non-auditory percepts. With the penetrating electrodes, she achieved gap detection thresholds of 2 to 10 ms, which suggest very good temporal resolution.

The patient also had been implanted with an array of electrodes on the surface of the cochlear nucleus, and the auditory percepts were quite different for the surface and penetrating electrodes. In general, the penetrating electrodes produced sounds closer to pure tones (described as being like chimes or a calliope), which she found distracting, at least at first. However, by day 3, she apparently had begun to integrate the percepts from the surface and penetrating electrodes, and by using a combination of 7 surface and 5 penetrating electrodes, she was able to achieve consonant and vowel recognition scores of 30- 35%, and modest open-set recognition of words in sentences (14%), which is exceptional performance for an ABI patient during initial testing. These results indicate that the targeting of the penetrating array into the cochlear nucleus was good at the time of surgery, that the array was inserted fully and stayed in place, and that the penetrating electrodes did not damage the neurons in the cochlear nucleus.

A second objective of this project is to develop central auditory prostheses based on an array of microelectrodes implanted into the ventral cochlear nucleus, in order to restore hearing to patients in whom the auditory nerve has been destroyed bilaterally. Our contract calls for the development of arrays of silicon substrate electrodes, which should allow placement of many more electrode sites into the human ventral cochlear nucleus than is possible with discrete iridium microelectrodes. We are developing an array for implantation into the human cochlear nucleus which has 16 electrode sites distributed on 4 silicon shanks extending from an epoxy superstructure that is 2.4 mm in diameter.

The probe shanks are either 2 or 3 mm in length. The 3 mm probes are intended to span the full tonotopic gradient of the human ventral cochlear nucleus, while the 2 mm shanks are appropriate for implantation into the feline ventral cochlear nucleus. To date, three of the 2 mm arrays have been implanted into the posteroventral cochlear nucleus 3 young adult female cats.

An electrode array with 2 of the 2-mm probes was implanted into the cochlear nucleus of a young male cat. In two previous animals, the array was implanted at a high angle (close to the vertical) so that the silicon shanks would traverse the isofrequency lamina of the ventral cochlear nucleus at a steep angle. In the present cat (CN145), the array was implanted into the dorsolateral surface of the nucleus at an angle of about 30° from the vertical, to allow the

underside of the array to lie nearly flat on the sloped dorsolateral surface of the nucleus, rather than having the lateral surface of the array elevated off of the nucleus. Also, experience with the first 3 human patients who were implanted with the arrays of discrete iridium microelectrodes indicates that this will be the preferred method of implanting these penetrating arrays.

The neuronal activity induced by 8 of the silicon sites was mapped in the contralateral inferior colliculus by recording the compound action potentials evoked by a stimulus current of 20 μA in the ventral cochlear nucleus (biphasic, controlled-current pulses of 150 μs/phase). Recordings were made at intervals of 100 μm along the dorsolateral to ventromedial axis of the IC, between the surface and a depth of 4,800 μm. The source of neuronal activity was localized using current source density analysis. The results of this analysis were consistent with the cochleotopic organization of the feline cochlear nucleus as demonstrated previously by other workers, using anterograde tracers injected into the cochlea. We showed that access to the tonotopic axis of the cochlear nucleus still is possible with the low-angle approach, particularly in the caudal part of the nucleus (the posteroventral cochlear nucleus). However, with this orientation of the silicon shanks, there is significant overlap of the frequency bands excited by adjacent electrode sites on a particular shank. Also, more than one shank will be required to access the entire tonotopic axis.

I: Results from patient #2 with the penetrating auditory brainstem implant (PABI)

The second PABI patient was implanted in November 2003 and initial stimulation occurred January 13-16, 2004.

The patient was a 42 year old female with type II neurofibromatosis who had her left-side vestibular schwannoma (VS) removed in 1984. Although she only had a small VS at that time in the right side, she was profoundly deaf. She received a cochlear implant on the right side in 1988 and achieved functional hearing (limited phone conversational use) for more than 15 years. Starting in 1999-2000 she experienced a decline in the hearing provided by the cochlear implant and it was removed in 2003 prior to an MRI.

PAB patient I#2 received both a surface electrode array and a penetrating electrode array following right VS removal in November 2003. At the surgery the anatomical landmarks were clearly identified and the penetrating array was inserted at the base of the remaining VIII nerve stump, inferior to the edge of the taenia. Both at the time of surgery and at a post-op review meeting, the entire ABI team concurred that the surgical placement was in the desired location. The patient recovered without difficulty and was discharges from the hospital four days after surgery.

PABI#2 returned for initial stimulation on Jan 13, 2004. A physician was on hand and continuously monitoring vital signs (blood pressure and heart rate) during the initial stimulation of the penetrating PABI electrodes. A crash cart and defibrillator was available in the room. No changes in vital signs were observed during stimulation with the penetrating electrodes and no unexpected non-auditory side effects were observed.

Threshold and Dynamic Range

Thresholds were measured using 250 pps stimulation for 400 ms. Surface electrodes were stimulated with 300 us/phase biphasic pulses, while penetrating electrodes were stimulated with 25 or 62 us/phase biphasic pulses. Figure 1-1 presents threshold and upper levels of comfortable loudness (MCL) measures in terms of charge, to compensate for the different pulse durations. Auditory thresholds were obtained on all 14 surface electrodes and on 7 of 8 penetrating electrodes. MCLs were obtained on most electrodes, but some produced non-auditory side effects (NASE) in addition to sound sensation at higher loudness levels. Seven of the 14 surface electrodes and 5 of the penetrating electrodes produced a full range of loudness without NASE. Most occurrences of NASE consisted of a tingling or vibratory sensation in the ipsilateral eye or in the vicinity of the ipsilateral ear canal. In one case the sensation was painful (surface electrode 20) and so stimulation was discontinued. On two penetrating electrodes (P13 and P16) she reported a dizzy feeling. Dizziness was not reported on electrode P16 on any of the following days of testing.

Note that the threshold measures from the penetrating electrodes indicate that the penetrating electrodes were indeed in the cochlear nucleus. Thresholds were between 1 and 3 nC for most penetrating electrodes and below 1 nC for two electrodes. These threshold levels compare favorably with those obtained in animals with penetrating electrodes, and are a factor of 10 lower than thresholds on surface electrodes.

Pitch

One of the primary goals of penetrating electrodes was to provide access to the tonotopic layers deep to the surface of the VCN. The perceptual consequence of this would be that the penetrating electrodes should produce a large range of pitch sensations. Figure 1-2 shows pitch estimation for stimulation of six of the penetrating electrodes as a function of their length. In general shorter electrodes produced high pitch sensations and long electrodes produced low pitch sensations. Subjectively PABI#2 reported that electrode P16 produced a deep base pitch like a base drum, while electrode P7 produced a pleasant high-pitch sound like the highest key on a piano. Figure 1-3 shows the distribution of pitch across the penetrating electrode array. We had expected the reverse pitch mapping – high pitch sensations from long electrodes penetrating deep to the surface. It is not completely clear why we observed the reverse pitch order, but it may be due to the different angle of penetration into the nucleus. Our original insertion tool design contained an angled tip to allow the microelectrodes to penetrate from into the ventral cochlear nucleus from its ventral surface. That angled tip was straightened due to the difficulty of maneuvering it in the narrow surgical opening and the ability of the surgeon to angle the tool with a straight barrel. The achieved insertion angle is more medial and less superior than the original plan and it is possible that we are penetrating the tonotopic strata "from the side" relative to our original plan. We will continues to check the consistency of the tonotopic mapping in the next PABI patients and will have anatomist Jean Moore review the tonotopic anatomy relative to the pitch ranking results, to achieve a more definitive explanation.

Intensity Discrimination

Intensity difference limens (DLs) were measured for one penetrating electrode (P16) as a function of the stimulation level. The results (Figure 1-4) show that PABI#2 could detect a change of intensity of 20-25% regardless of the loudness of the standard stimulus. While this DL is large compared to cochlear implants, it is similar to DLs observed in previous ABI patients with surface electrodes and indicates that she should be able to discriminate only 4-5 steps in intensity across the dynamic range. Limited testing time did not allow further intensity DL measures.

Gap Detection

One measure of temporal resolution is the ability to hear a silent gap in an ongoing stimulus. PABI patient #1 had relatively long gap detection thresholds (reported in the last QPR) as 50-100 ms. Figure 1-5 shows gap detection thresholds for two electrodes (surface S12 and penetrating P16), for PABI patient #2. For the penetrating electrode, she was able to detect gaps of 2-10 ms, which is well within the range expected for normal hearing listeners or cochlear implant listeners. The upper panel of Figure 1-5 shows gap detection thresholds from previous patients with surface electrode ABI devices and the hatched area shows the range of gap detection thresholds from 38 cochlear implant listeners. For the surface electrode, gap detection thresholds for PABI patient #2 decreased from about 50 ms for soft sounds to about 15 ms for medium loudness sounds, again both values close to those observed for normal hearing listeners and cochlear implant listeners.

Speech Recognition

PABI#2 was fit with three speech processors: one using seven surface electrodes (S7), one using 5 penetrating electrodes only (P5), and one using all 12 electrodes combining surface and penetrating electrodes (S7+P5). For each processor the threshold and comfortable loudness level was determined for each electrode. Then the electrodes were ordered in terms of pitch. Typically all electrodes were played at equal loudness and the subject was asked to select the one that was the lowest pitch. That electrode was then removed from the set and the set played again. The subject was now instructed to select the highest-pitch electrode. This process continued until all electrodes had been selected. Then all electrodes were played at equal loudness in what should be the correct pitch order. If ambiguities exist of irregularities noted, electrodes that were similar in pitch were played sequentially multiple times and the subject was instructed to select which was higher in pitch. Once the pitch order was determined, the frequency rang was divided into approximately equal logarithmic steps and each acoustic frequency band was assigned to successive electrodes in pitch order. Several frequency range assignments were tried to see if one might produce better sound quality or phoneme discrimination than another. Testing for this iterative phase was done with numbers and with spondee words all presented by live voice. At initial fitting PABI#2 remarked that the penetrating electrode map sounded whistling – like a circus calliope, suggesting that the distinct pitch sounds from the different electrodes were not fusing into a single perceptual image. She reported that the surface electrode map was pleasant and natural sounding, much like she remembered from her previous experience with her cochlear implant. The combined map containing both surface and penetrating electrodes produced a dual sound sensation that she described as “someone talking and a bunch of chimes”. Again this suggests that, at least initially, she was not integrating the sound quality from the penetrating electrodes with the surface electrodes. Presumably the penetrating electrodes were producing what she described as “chimes” and to her this sound was “on top of” the voice sound, even interfering with the speech understanding. After a day of practice with the combined map this dichotomy decreased and there was some indication that she was starting to integrate the two sound sources. Formal speech tests conducted on day 3 (Figure 1-6) show a synergistic effect of surface and penetrating electrodes - even with only a few days of experience she was able to recognize speech better with the combined map than with either surface or penetrating maps alone. Figure 1-6 shows results from three speech processors on recognition of medial vowels and medial consonants and simple sentences (CUNY) using only the sound from the PABI device and no lipreading. While she was able to recognize vowels and consonants at a level above chance, the combined map allowed recognition at 35-40% correct, a level that will begin to allow open set speech understanding. Indeed, PABI#2 was able to recognize 14% correct words in sentences in the sound alone condition. This is the first time we have observed this level of performance at initial stimulation in more than 150 patients with auditory brainstem implants. At this point it is not clear if this excellent performance is due to her prior experience with a cochlear implant (and thus experience with minimal and possibly distorted speech cues) or to an immediate ability to use the pitch information from the penetrating electrodes.

Evoked Response Measures

Intraoperative electrically-evoked auditory brainstem responses (EABRs) were recorded from scalp electrodes during stimulation with both surface and penetrating electrodes in PABI patients #2 and #3. In PABI patient #2, post-operative EABRs were also recorded while

stimulation with both penetrating and surface electrodes. No EABRs were observed while stimulating with the penetrating electrode in PABI#2, either intraoperatively or postoperatively. Clear stimulation artifacts were observed during the postoperative testing, indicating that stimulation was being delivered to the electrodes properly. However, even though auditory perception was achieved for seven of the eight penetrating microelectrodes, no EABRs were obtained that were reliable. A postoperative EABR from at least one surface electrode was observed and had a waveform morphology that was similar to that recorded during stimulation with the same electrode during surgical placement. In PABI patient #3, EABRs evoked from most of the surface electrodes were recorded intraoperatively but no reliable EABRs were observed while stimulating with most of the penetrating electrodes. A small EABR from one penetrating electrode was detected intraoperatively, but we will not know until initial stimulation (Mid-March 2004) if that electrode produces auditory sensations. In general, it appears that intraoperative monitoring of EABRs is effective for assistance in positioning the surface ABI array, but may not be as useful for assisting the placement of the penetrating array. We will continue to measure intraoperative and post-operative EABRs from penetrating electrodes in an attempt to improve recording parameters and techniques.

Post-Operative Imaging

In PABI patient #1 we attempted to document the location of the PABI electrodes using interleaved CT imaging sequences with double contrast. Although CT images do not show soft tissue structures, we have shown in the past that it is possible to determine if surface ABI electrodes are in the vicinity of the lateral recess of the IV ventricle by assessing their location relative to bony landmarks. Repeated imaging sequences over time can show movement of electrode assemblies relative to bony landmarks. Unfortunately, we were unable to visualize the penetrating electrodes of the PABI in CT images in PABI#1.

In PABI patient #2 we tried to document/quantify the location and orientation of the penetrating electrode assembly using standard views with high resolution plain film X-rays. The images did have sufficient resolution to see the individual microelectrodes in the penetrating array and the relative position and orientation of the array could be documented. We hope to repeat such images in subsequent PABI patients to see if they can provide verification of good vs poor electrode placement and to verify electrode stability over time.

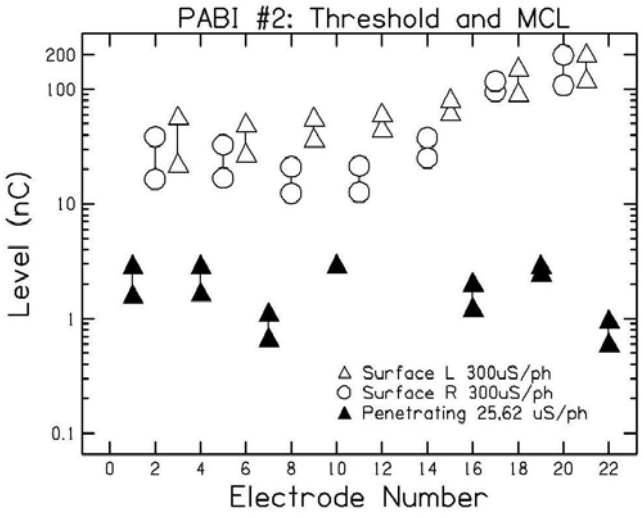

Figure 1-1

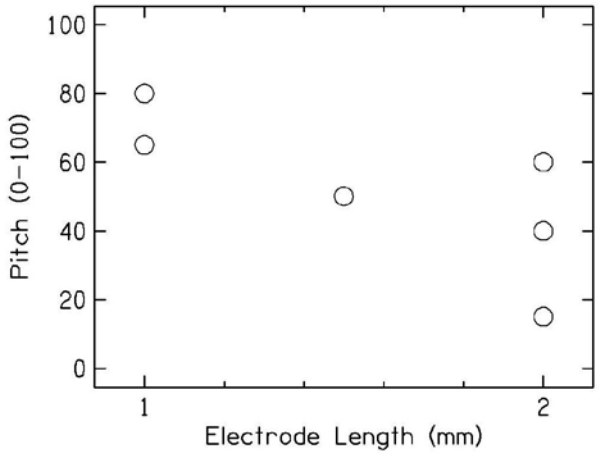

Figure 1-2

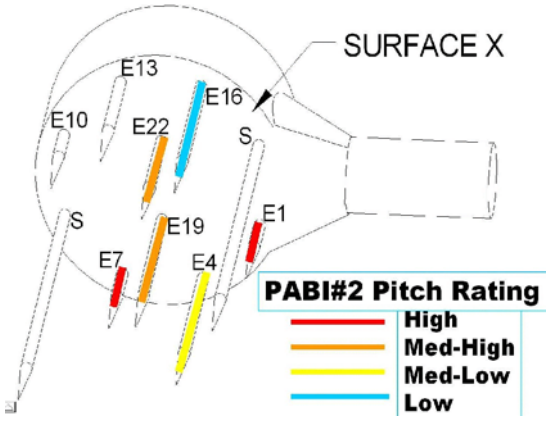

Figure 1-3

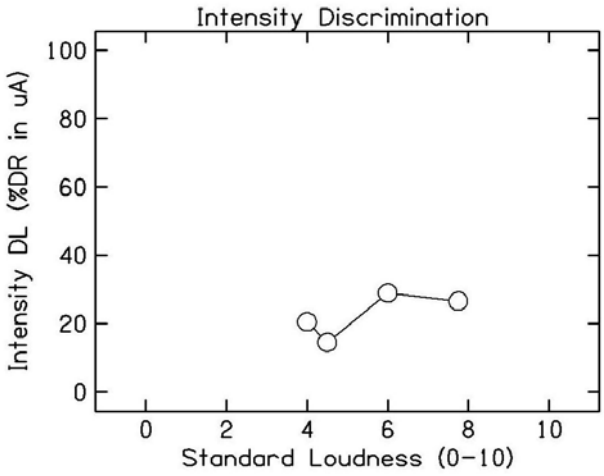

Figure 1-4

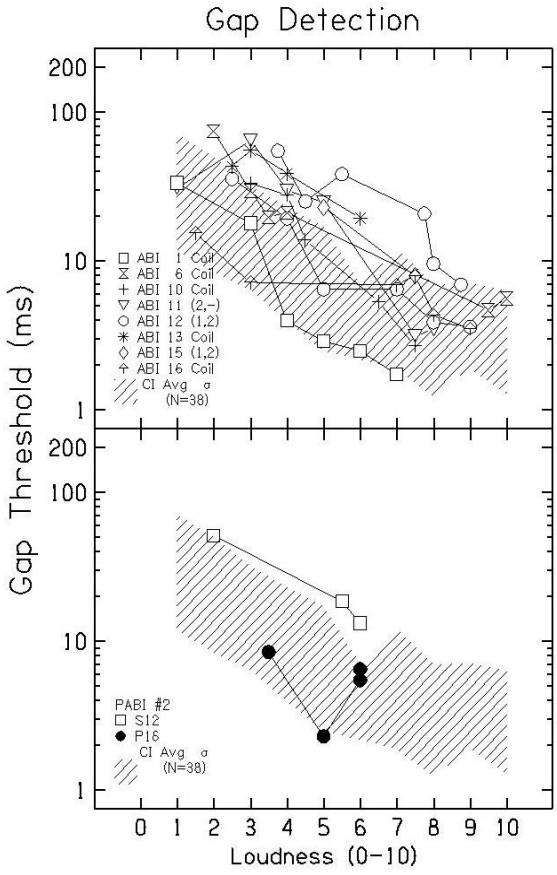

Figure 1-5

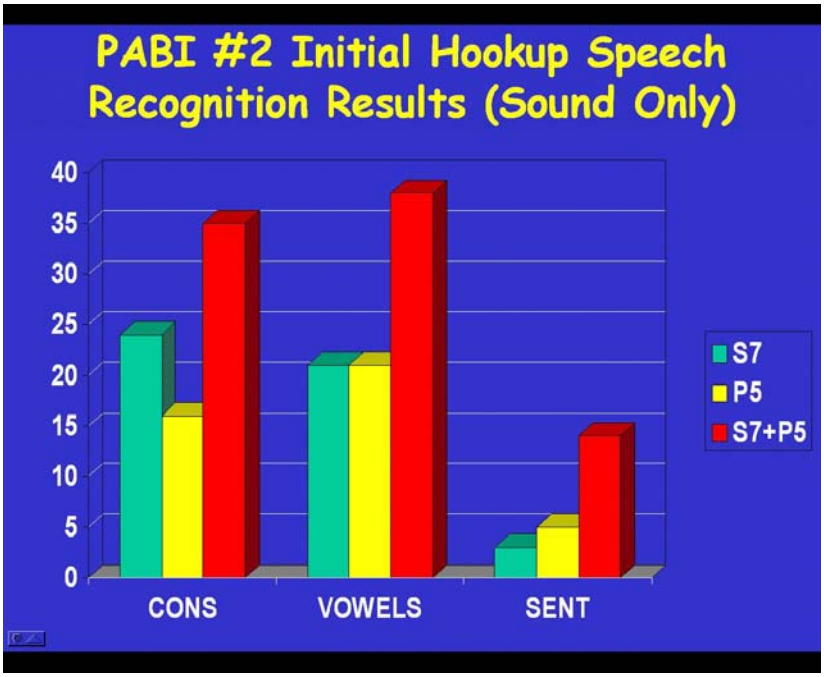

Figure 1-6

2: Development of an array of silicon substrate microelectrodes
METHODS

The objective of this project is to develop central auditory prostheses based on an array of microelectrodes implanted into the ventral cochlear nucleus, in order to restore hearing to patients in whom the auditory nerve has been destroyed bilaterally. Our contract calls for the development of arrays of silicon substrate electrodes, which should allow placement of many more electrode sites into the human cochlear nucleus than is possible with discrete iridium microelectrodes. We are developing an array for implantation into the human cochlear nucleus that has 16 electrode sites distributed on 4 silicon shanks extending from an epoxy superstructure that is 2.4 mm in diameter. This is the same footprint as our first- generation human arrays employing discrete iridium microelectrodes and is designed to be implanted using the same inserter tool. The silicon probes are fabricated at the University of Michigan under the direction of Design Engineer Jamille Hetke. Figure 2-1 shows an array with 2 of the probes (4 shanks and 16 electrode sites) extending from an epoxy superstructure that floats of the surface of the cochlear nucleus. The cable is angled vertically, to accommodate the transcerebellar approach to the feline cochlear nucleus.

We implanted an array of 16 silicon substrate electrodes into the ventral cochlear nucleus of cat CN145 . This array has 2 of the 2 mm probes (Array CN-Mich-6) . Several of the electrode sites were open-circuit before the implant procedure. This probably is due to the problem of delamination of the gold overlayer on the bonding pads, that we had noted previously.

Using aseptic technique, the scalp was opened in a midline incision, and the muscles reflected. A small craniectomy was made over the right occipital cortex and the bipolar recording electrode was introduced into the rostral pole of the right inferior colliculus. The reference electrode was dorsal to the colliculus. These electrodes are solid 100 µm ss wire, with ~ 1 mm of the Teflon insulation removed for the tips.

To access the cochlear nucleus, a craniectomy was made over the left cerebellum, extending up to the tentorium. In previous animals, we had inserted the arrays into the cochlear nucleus in a near dorsal-ventral orientation, so that the electrodes would cross the isofrequency lamina at a steep angle. In this animal, we elected to inert the array at angle of approximately 30 degrees from the vertical. This was done so that the array could be inserted into the lateral wall of the cochlear nucleus and the underside of the array superstructure would be nearly parallel to the dorsolateral surface of the nucleus, which slopes at a steep angle. As noted in Part 1 of this report, our experience from the first two human patients suggest that it will be preferable to insert the arrays into the lateral surface of their ventral cochlear nuclei. To accommodate the low insertion angle, the craniectomy was extended laterally until we reached the large bone sinus. Part of the tentorium also was removed, to allow better access to the nucleus.

The rostrolateral portion of the left cerebellum was aspirated using glass pipettes. The electrode array was secured on the end of a vacuum wand, and thereby advanced into the cochlear nucleus. Note that this was a slow insertion.

Before releasing the vacuum, the array cable was fixed to the bone at the margin of the craniectomy, using medical grade SuperGlue (Figure 2-2) and the cavity was filled with gelfoam. After the procedure, with the cat still anesthetized, I recorded a good evoked responses response in the right inferior colliculus, in response to both acoustic and electrical stimulation.

Shortly after the surgery, and after the endo-tracheal tube was removed, the cat went into respiratory arrest. This apparently was due to a viscous mucus plug in the trachea. By the time he could be re-intubated, he has sustained about 3-4 minutes of anoxia. By the evening of the following day, he remained semi-conscious and was breathing on his own, and with normal-appearing evoked responses in the inferior colliculus. Because the animal's medical condition raised concerns that he would subsequently experience considerable duress if and when he recovered consciousness, we elected to perform a terminal experiment in which we mapped the projection of the various electrode sites into the contralateral inferior colliculus.

It is well established that high and low acoustic frequencies from the basal and apical cochlea map onto a dorso-to-ventral tonotopic gradient in the ventral cochlear nucleus and that this ordered representation of acoustic frequencies then projects (in an inverted manner) onto the central nucleus of the inferior colliculus, with low acoustic frequencies represented in the dorsolateral part of the IC's central nucleus and high frequencies in the ventromedial portion.

The inferior colliculus mapping was done with the cat anesthetized with isoflurane and oxygen. The stimulus current was 20 μA, with a 150 μs/phase duration, at 50 Hz. The response from electrodes sites 1,3,5,7,9,10,11 and 13 in the ventral cochlear nucleus were mapped at 100 μm increments of depth along the dorsolateral-ventromedial axis of the IC, from the surface to a depth of 4.8 mm. The responses from all 8 sites was acquired before the depth of the recording electrodes was advanced. The response to 512 successive stimuli were averaged, at each depth in the IC and for each electrode site in the CN.

Current source density (CSD) analysis has been shown to be useful for localizing coherent induced neural activity. The technique locates regions within the tissue volume in which current is passing from the extracellular compartment into (or out of) a spatially extensive intracellular compartment. The CSD at point x,y,z within the tissue volume represents the net current flowing in or out of the neural elements and is given by:

$$I_{d(x,y,z)} = -[\ \sigma_x\ \delta^2\ \phi/\delta x^2 + \sigma_y\ \delta^2\ \phi/\delta y^2 + \sigma_z\ \delta^2\ \phi/\delta z^2\ ] \quad (1)$$

where ϕ is the field potential at x,y,z, and σ_x, σ_y and σ_z are the principal tissue conductances (Freeman and Nicholson, 1975). To compute equation 1, the extracellular field potential must be measured simultaneously at 7 (or more) points, at and around x,y,z. However, in situations in which the neuronal responses to the stimulation are quite constant over time and in which the tissue is nearly isotropic ($\sigma x \cong \sigma y \cong \sigma z \cong \sigma$) as in the central nucleus of the inferior colliculus (Harris, 1987), then the current source density can be computed from measurements of the averaged evoked potential obtained along a single axis. Freeman and Nicholson (1975) compared various smoothing procedures for reducing the noise inherent in the calculation of the 2nd spatial derivative of ϕ, while maintaining the essential spatial resolution. The 5-point finite approximation appeared to be the most useful:

$$I_{d(x,y,z),} \cong D(x,y,z) = (0.01\ \sigma/h^2)[-2\phi(x-2h)\ -\ \phi(x-h)\ -\ 2\phi(x) + \phi(x+h)\ +\ 2\ \phi(x+2h)] \quad (2)$$

Here, h is the spacing between the points at which the instantaneous field potential ϕ is measured. This formula is computationally equivalent to obtaining a least-squares error fit of a cubic polynomial to 5 successive data points along the axis of measurement, and then computing the second derivative of the fitted polynomial. We have used this versions of CSD to demonstrate that intranuclear microstimulation with discrete iridium microelectrodes can

access the tonotopic gradient (McCreery el al, 1998). We did not measure the conductivity of the living tissue in the inferior colliculus, and therefore, the CSD is expressed as arbitrary units.

RESULTS

The diagram in Figure 2-3 shows the locations of the electrode sites on the 4 shanks of the array implanted into this cat. Figures 2-4A-D show the compound action potentials evoked from each of the 4 sites on the rostral lateral shank (sites 1,5,9 & 13) as a function of depth in the contralateral IC. Site 1 (Figure 2-4A) was closest to the surface of the cochlear nucleus, and site 13 (Figure 2-4D) was deepest. Although we were not able to perfuse the cat at the end of this experiment, and thus we were not able to determine the precise locations of the probe shafts, we were able to determine that this shaft was slightly rostral of the place of entry of the 8th nerve, and thus in the caudal part of the anterioventral cochlear nucleus. For all 4 sites on this shank, the evoked potentials are greatest deep in the IC, in the region representing high acoustic frequencies. Figure 2-5 shows the potentials evoked from electrode site 10, the only functional site on the rostromedial probe. Figure 2-6A-C show the depth profiles of the potentials evoked from electrode sites 3, 7 & 11 on the caudal medial shank, which was close to the caudal pole of the nucleus and well within the medial part of the PVCN.

Current source density analysis allows better localization of synchronous neuronal activity that is possible from the field potentials alone (Freeman et al., 1975).
Current sinks (negative values of CSD) occur when membrane depolarization causes ionic currents to flow into a neuron. Current sinks are commonly equated with regions of excitatory synaptic activity. Under these conditions, the spatially adjacent current sources represent the return of this current to the extracellular compartment, through passive membrane. Sinks also may be generated by synchronous action potentials, wherein the spatially adjacent current sources represent the return of the current to the extracellular compartment through passive neuronal membrane, and the temporally adjacent sources represent repolarization of the active neuronal membranes. However, current sources also may be generated by inhibitory post-synaptic activity (ipsp's), with the associated sinks representing passive inflow of this current.

Figure 2-7A shows the depth profile in the IC of the compound potentials evoked from electrode site 3. Figure 2-7B shows the corresponding depth profile of the CSD, as computed from the potentials shown in Figure 2-7A, using equation 2. Figures 2-7C and D show the contour plots of the potential and CSD profiles, respectively. Current sinks are shown in red or magenta, and sources are shown in blue or black. Note that the CSD affords better localization of the regions of neuronal activity.

Figure 2-8A - D are the contour plots of the CSD depth profile for electrode sites 1,5,9 & 13 on the rostrolateral shank, as computed from the potentials shown in Figure 2-4. While there is a tendency for the current sources evoked from electrode sites deeper in the cochlear nucleus to occur at a shallower depth in the IC, all of the active current sinks are located deep in the IC. The sinks evoked from electrode site 10 on the adjacent rostromedial shank also were very deep in the IC and, in fact, deeper than the sinks evoked from site 9 , the corresponding site on the rostrolateral shank. Since the medial shank was more dorsal in the nucleus, this relation is consistent with the known tonotopic organization of the VCN.

Figure 10A-C show the current sources and sinks evoked from electrode sites 3,7 & 11 on the caudal-medial shank. In this case, the current sinks evoked from the different electrode sites in the PVCN do span most of the depth of the dorsolateral- ventromedial axis of the IC.

DISCUSSION

The results of this experiment can best be appreciated in the context of work done by Russ Snyder and Pat Leake and their colleagues at the University of San Francisco. (Snyder et al , 1997; Snyder and Leake ,1997). They examined the tonotopic organization of the primary afferent projections to the cochlear nucleus in adults and in immature cats, using focal extracellular injections of Neurobiotin (NB) into the spiral ganglion of the basal cochlea. One to three injections separated by intervals of at least 2 mm were positioned along the basal one-third of the cochlea. Each injection produced discrete projection laminae of labled afferent axon terminal that correspond to the a narrow band of acoustic frequencies ("oligofrequency laminae"). These were distributed sequentially, dorsally- to- ventrally, across each major CN subdivision: the anteroventral, posteroventral, and dorsal cochlear nucleus, (AVCN, PVCN, and DCN, respectively).

Figure 2-11 shows two illustrations from their work, with my added sketches of an electrodes array inserted into the dorsolateral surface of the nucleus. The Neurobiotin labeling representing the oligofrequency lamina (each representing a different injection site in the cochlea) are shown as dark bands. In our cat CN145, the microstimulating array was inserted into the dorsolateral surface of the ventral cochlear nucleus. In the caudal part of the VCN, in the PVCN (left panel of Figure 2-11), the oliofrequency laminae are nearly planar and are inclined with respect to the dorsolateral surface of the nucleus. Thus a silicon shank that is nearly perpendicular to the dorsolateral surface of the nucleus would be expected to traverse a significant portion of the tonotopic strata and stimulating sites close to the superstructure of the array would be expected to excite high-frequency neurons in the PVCN which project to sites deep in the IC (and vice- versa for sites near the tips of the probe. This is what is shown in figure 2-10. However, because the shanks cross the tonotopic strata obliquely, more than one probe will be required to gain access to the entire tonotopic gradient of the PVCN, and the overlap of regions subserving similar acoustic frequencies that are excited by adjacent sites along each probe would be greater than would be the case if the probe were inserted in a more dorsal- to-ventral orientation. In humans, the electrodes most likely will penetrate into the PVCN, since the AVCN is partly hidden beneath the middle cerebellar peduncle.

More rostrally, in the PVCN, the oligofrequency laminae also are arranged in a dorsal-high frequency, ventral-low frequency ordering, but the laminae tend to be oriented perpendicular to the dorsal surface of the nucleus, or to be somewhat cup-shaped (right panel of Figure 2-11). Thus, the tonotopic ordering of the response from stimulating sites distributed along a probe inserted into this region of the nucleus from the dorsal-lateral surface would be less predictable, and a portion of the tonotopic gradient that is accessed by any one probe would be quite limited. This is indeed what is shown in figure 2-8.

In summary, the neuronal activity induced by 8 of the silicon sites was mapped in the contralateral inferior colliculus by recording the compound action potentials evoked by the microstimulation in the ventral cochlear nucleus. The source of neuronal activity was localized using current source density analysis and the results were consistent with the cochleotopic organization of the feline cochlear nucleus as previously demonstrated by other workers using anterograde tracers injected into the cochlea. We showed that access to the tonotopic axis of the cochlear nucleus still is possible, particularly in the caudal part of the nucleus (the posteroventral cochlear nucleus). However, with this orientation of the silicon shanks, there is significant overlap of the frequency bands excited by adjacent electrode sites on a particular

shank. Also, more than one shank will be required to access the entire tonotopic axis. In the future, we will perform similar experiments using a range of stimulus pule amplitudes and pulse durations, and for different points of insertion of the stimulating array into the cochlear nucleus.

As we noted above, we have been experiencing persisting problems related to continuity between the lead wires and the bonding pads on the spines of the silicon probes. The contact failures occur during the fabrication process when there is considerable handling and manipulation of the lead wires rather than after implantation, where the probes have proved to be quite stable. Two corrective measures have been instigated. Firstly, the personnel at the Center for Neuronal Communications Technology have taken steps to improve the adhesion of the gold bonding pads to the underlying substrate. Secondly, extensively revised our proceedure for fabricating the arrays in order to reduce stress on the silicon substrate during the bonding of the lead wires to the probes. This modified procedure will be described in detail in the next quarterly progress report.

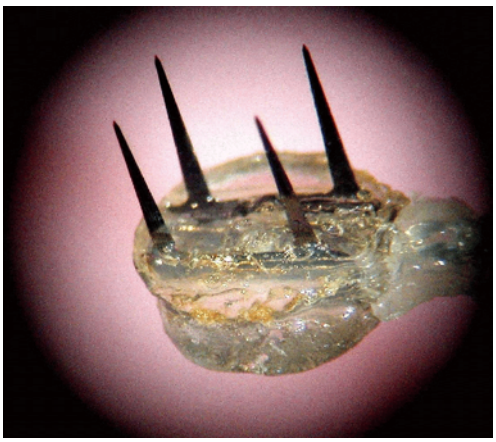

Figure 2-1

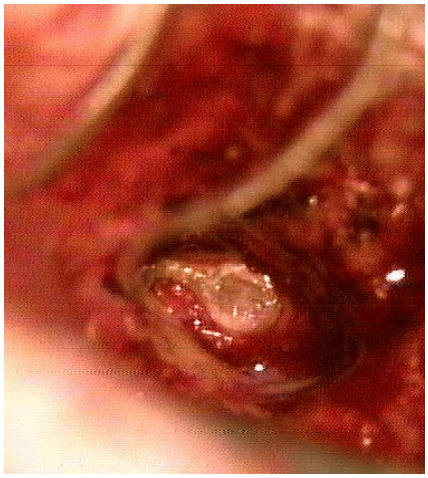

Figure 2-2

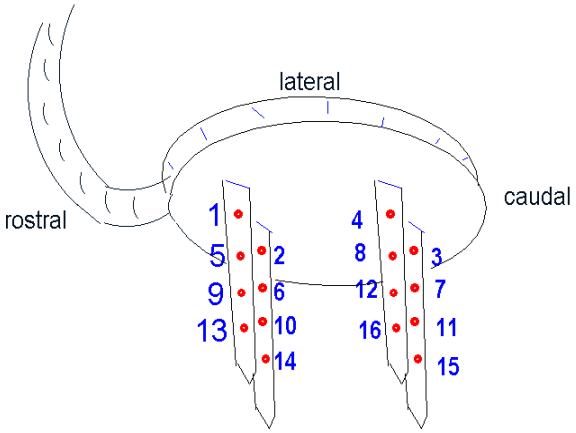

Figure 2-3

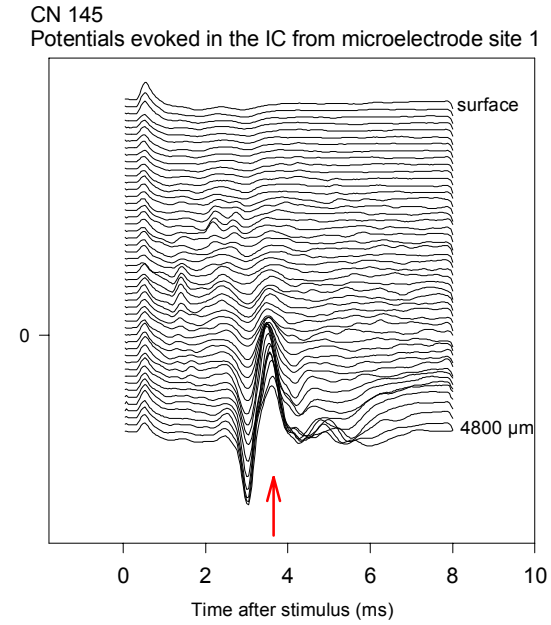

Figure 2-4A

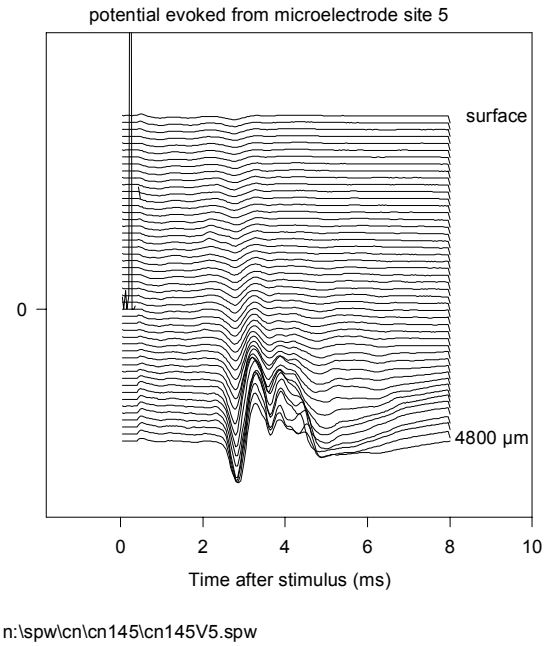

Figure 2-4B

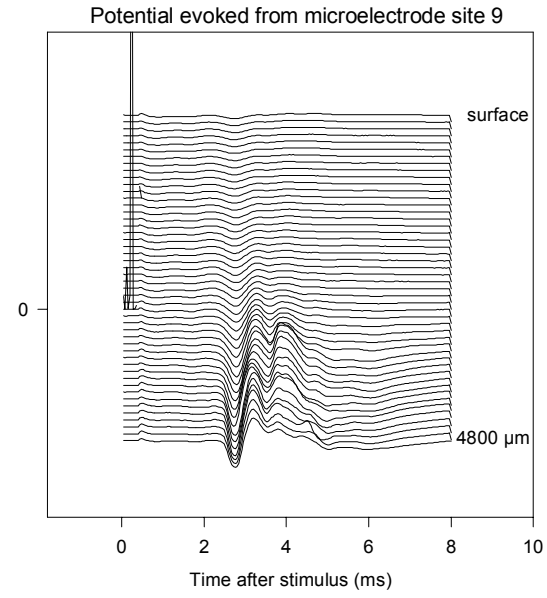

Figure 2-4C

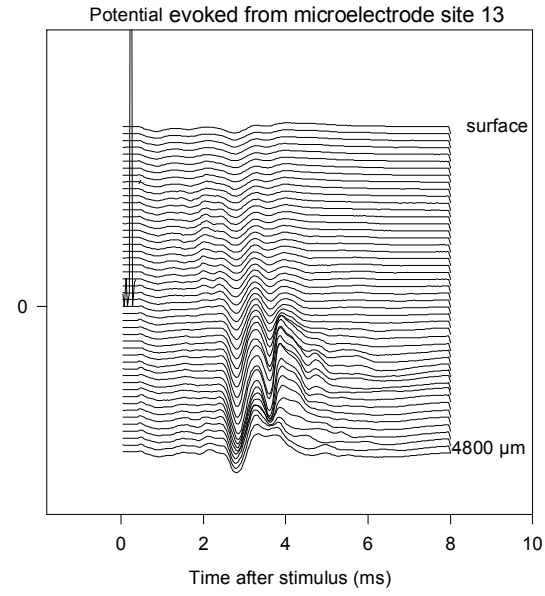

Figure 2-4D

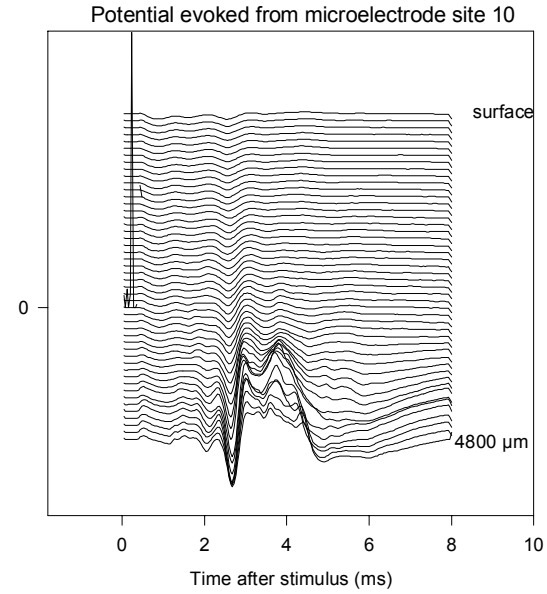
Potential evoked from microelectrode site 10
surface
4800 µm
0
0
2
4
6
8
10
Time after stimulus (ms)
n:\spw\cn\cn145\cn145V10.spw

Figure 2-5

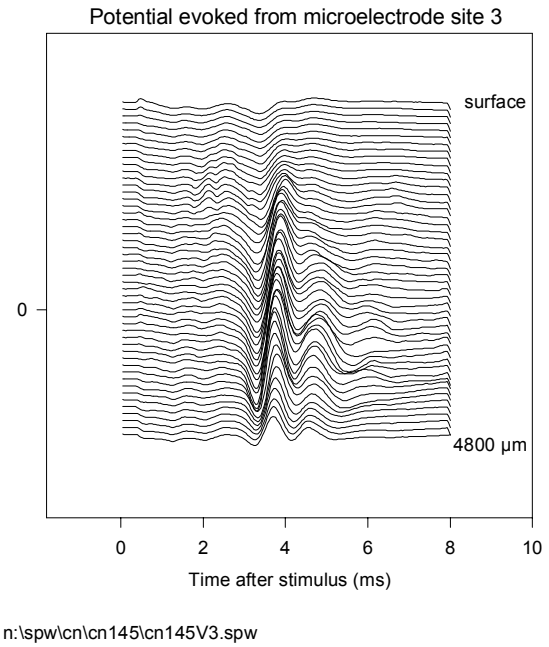

Figure 2-6A

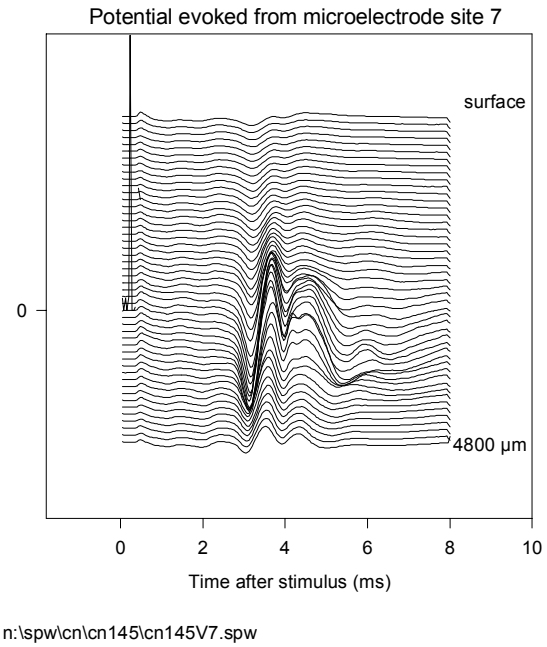

Figure 2-6B

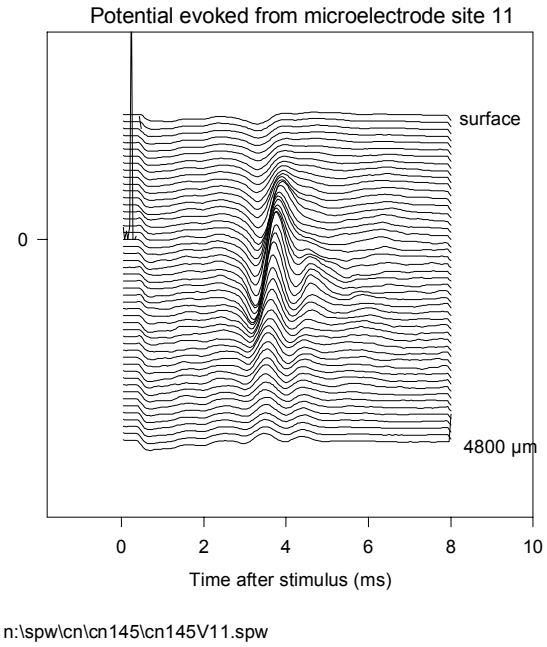

Figure 2-6C

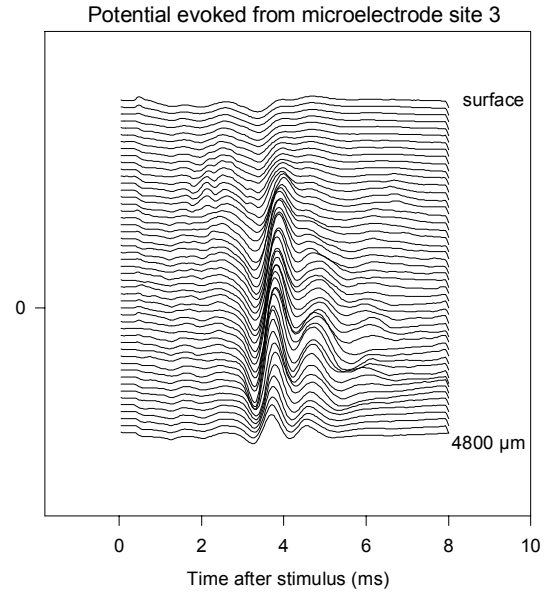

n:\spw\cn\cn145\cn145V3.spw

Figure 2-7A

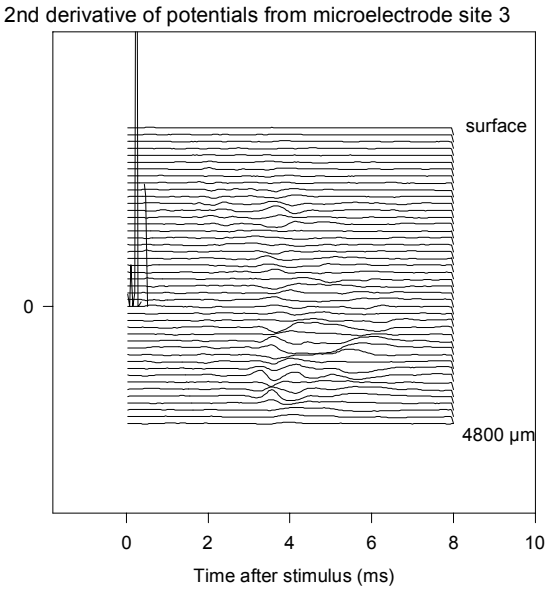

n:\spw\cn\cn145\cn145d3.spw

Figure 2-7B

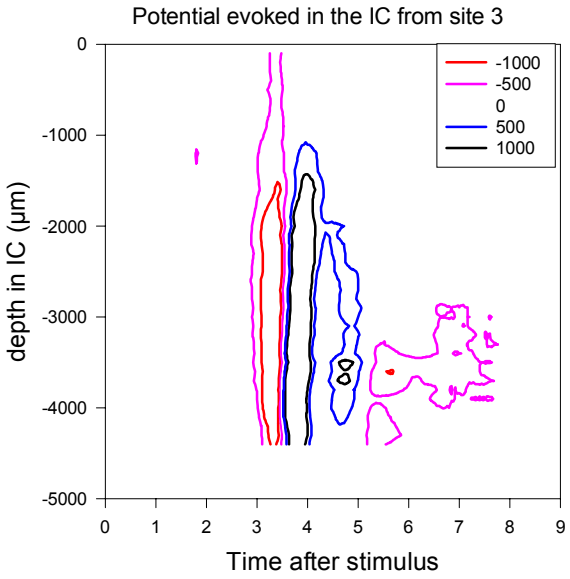

d:/spw/cm/cn145/pcont_3.spw

Figure 2-7C

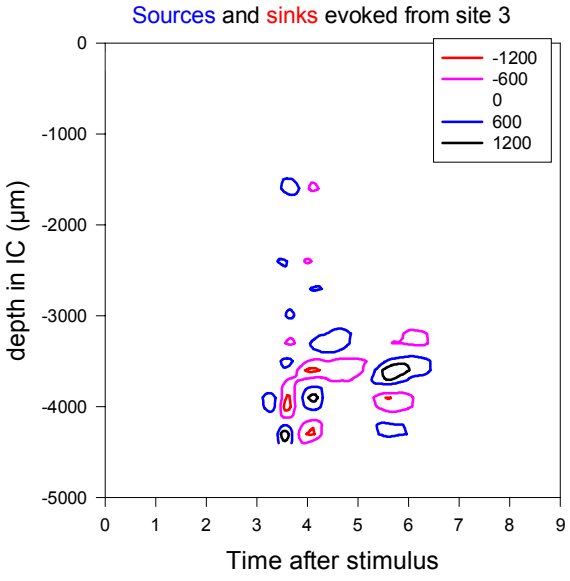

d:/spw/cm/cn145/cont_3.spw

Figure 2-7D

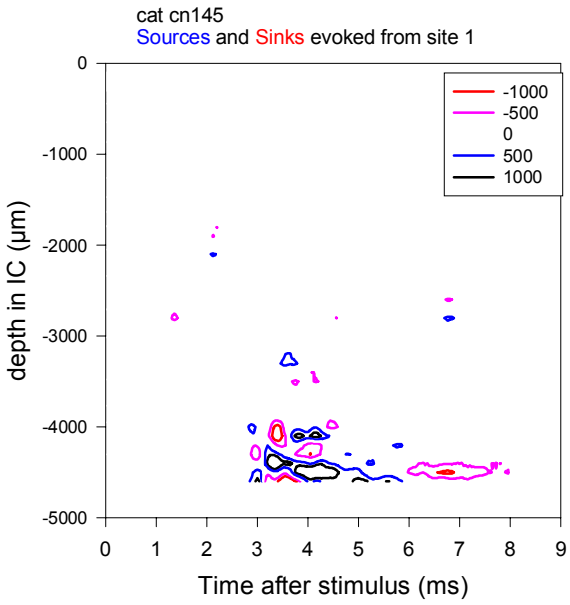

Figure 2-8A

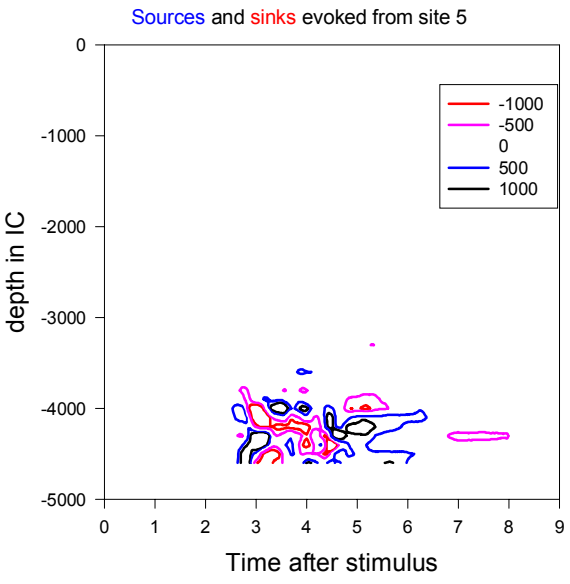

Figure 2-8B

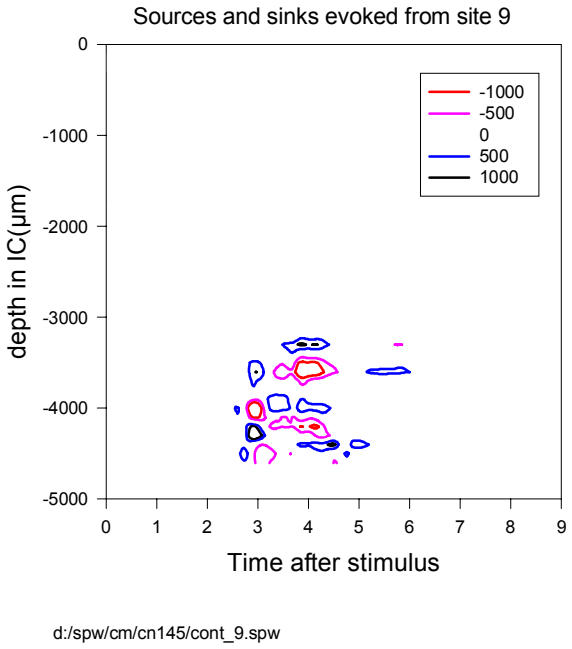

Figure 2-8C

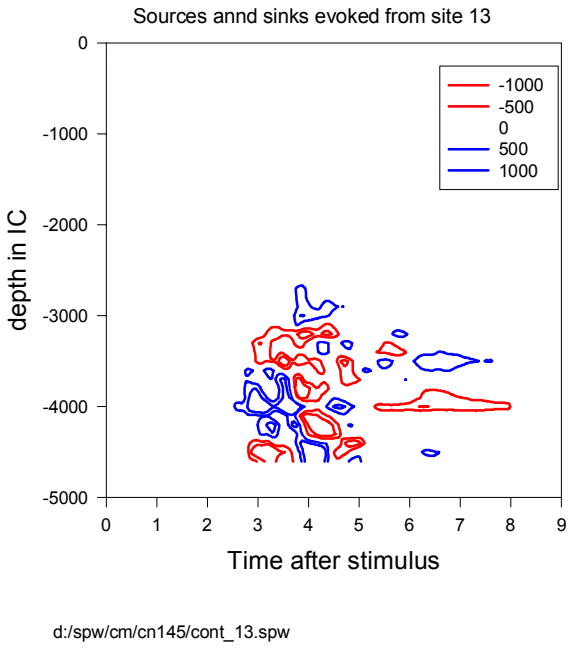

Figure 2-8D

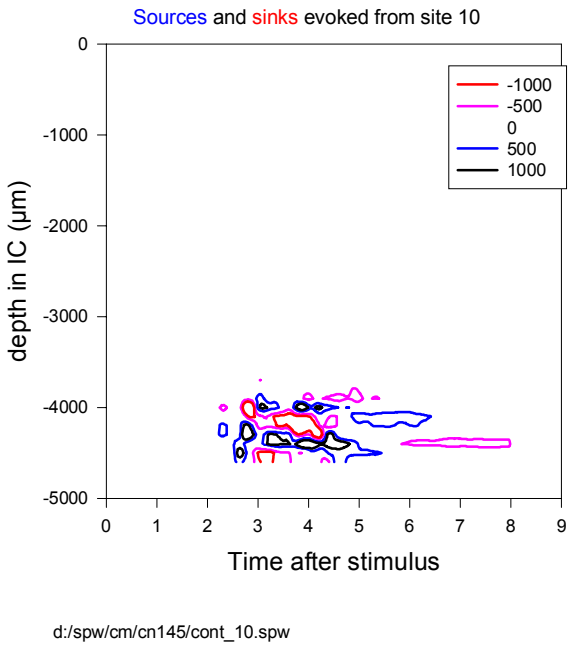
Sources and sinks evoked from site 10
0
-1000
-2000
-3000
-4000
-5000
depth in IC (µm)
0
1
2
3
4
5
6
7
8
9
Time after stimulus
-1000
-500
0
500
1000
d:/spw/cm/cn145/cont_10.spw

Figure 2-9

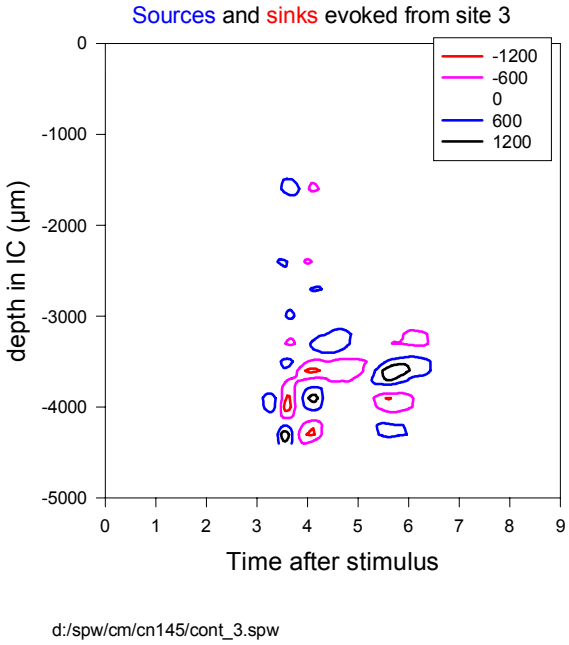

Figure 2-10A

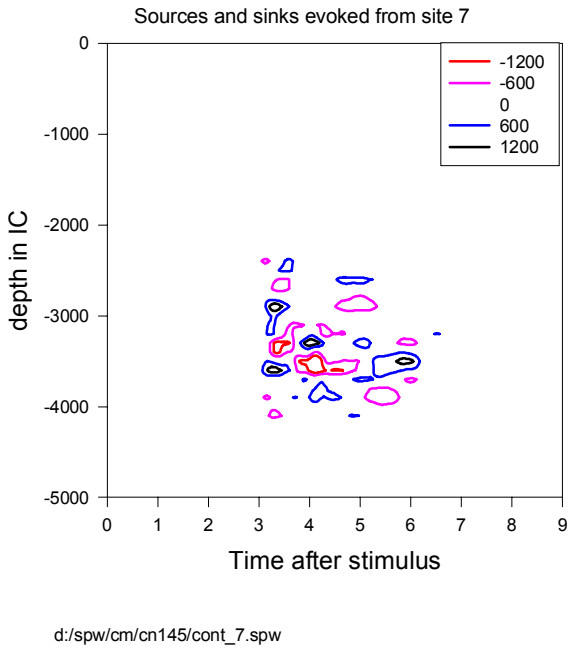

Figure 2-10B

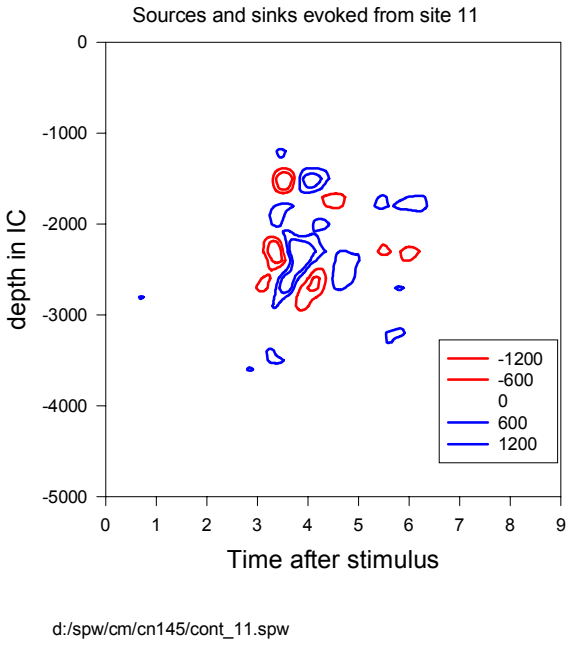

Figure 2-10C

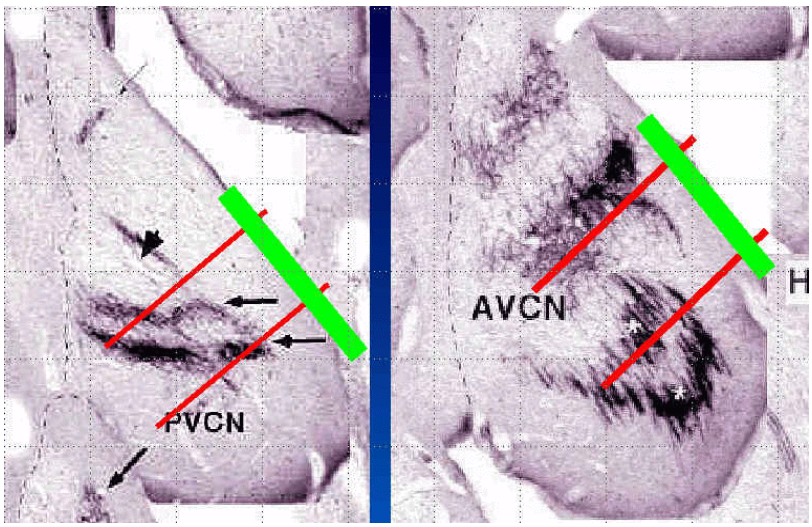

Figure 2-11 (Modified from Snyder, Leake and Hradek, 1997)

REFERENCES

J. A. Freeman and C. Nicholson, "Experimental optimization of current source-density technique for anuran cerebellum," *J Neurophysiol*, vol. 38, pp. 369-82., 1975

.

D. M. Harris, "Current source density analysis of frequency coding in the inferior colliculus," *Hear Res*, vol. 25, pp. 257-66, 1987.

D. B. McCreery, R. V. Shannon, J. K. Moore, and M. Chategee, "Accessing the tonotopic organization of the ventral cochlear nucleus by intranuclear microstimulation," *IEEE Transactions on Rehabilitation Engineering*, vol. 23, pp. 391-399, 1998.

R. L. Snyder and P. A. Leake, "Topography of spiral ganglion projections to cochlear nucleus during postnatal development in cats," *J Comp Neurol*, vol. 384, pp. 293-311, 1997.

R. L. Snyder, P. A. Leake, and G. T. Hradek, "Quantitative analysis of spiral ganglion projections to the cat cochlear nucleus," *J Comp Neurol*, vol. 379, pp. 133-49, 1997.